euspen's 25th International Conference & Exhibition, Zaragoza, ES, June 2025
www.euspen.eu

# Modeling of 3D surface topography during micromilling concerning the machined surface anomalies

Marcin Gołaszewski[1] Bartosz Powałka[1]

[1]*West Pomeranian University of Technology in Szczecin, Poland*

*Bartosz.powalka@zut.edu.pl*

**Abstract**
The reliable modeling of 3D surface topography during micromilling processes is up-to-date problem in precise manufacturing. However, the mechanisms of a machined surface anomalies constitution are still not recognized. Therefore, this work focuses on a modeling of 3D surface topographies during radial immersion micromilling concerning the machined surface anomalies induced by cutting force variations resulting from a geometry of the micro end milling cutter and tool-spindle system flexibility. The experiments involved radial immersion micromilling conducted with variable feed per tooth and radial depth of cut values, as well as the various milling kinematics (up-milling and down-milling). Results have shown that in down-micromilling process, carried out with tools equipped with a helical cutting edges and rounded corner radius, the formation of machined surface anomalies in a form of bands with the elevated machining marks towards the remaining area were observed. The proposed novel 3D surface topography model enables accurate estimation of geometrical parameters (heights and widths) of surface anomaly bands in a wide range of machining conditions, milling kinematics and tool geometries

micromilling; modeling; 3D surface topography; cutting forces; surface anomalies; helix angle

## 1. Introduction

In the theory, the surface topography after milling is affected by the so–called kinematic–geometric projection of the tool tip inside the workpiece, which considers the feed per tooth, pick feed, tool nominal diameter and corner radius. However, in micromilling practice, this theoretical model is characterized by a very low accuracy, since the machined surface topography is also significantly affected by the cutting forces, vibrations, geometrical errors of machining system (e.g. axial and radial run outs), tool microgeometry (and progressing tool wear), plastic/elastic deformations of a workpiece and other specific phenomena characterizing the micromilling process. Thus, the accurate and comprehensive modeling of a surface topography during micromilling is a great challenge and requires the development of a complex analytical/numerical models which include many factors characterizing the formation of a machined surface finish. An important group of factors included in models presented in a literature considers the basic physical phenomena appearing in micromilling (e.g. cutting forces and vibrations). According to Wang et al. [1], the cutting forces during milling have significant impact on the formation of a machined surface topography, since they contribute to the deflections of a tool tip. Cutting forces generated during milling processes induce the periodic deformations of a tool and/or workpiece and thus they can contribute to the generation of a surface location errors (SLE), or even the surface roughness, in case when the frequencies of force variations are higher than the frequency corresponding to feed per revolution. These findings were reported in works of Mann et al. [2] and Wojciechowski et al. [3]. The another highly undesirable phenomena affecting the deterioration of a surface finish are vibrations and process stability loss (resulting in generation of chatter). According to Grossi et al. [4], the generation of a high-amplitude chatter marks on the milled surfaces is affected by the so-called aliasing and pseudo moiré effects. Moreover – as reported by Kalinski and Galewski [5] – the instant tool tip deflections can induce the milling vibrations, which consequently relocate onto the machined surfaces and lead to the deterioration of a surface finish.

## 2. Surface topography model for micromilling process

In this study, the original 3D surface topography model based on a hybrid Homogenous Matrix Transformation / Z-Map (HMT/Z-Map), dedicated for a micromilling has been proposed. The formulated model tool tip trochoidal trajectory, as well as the geometrical errors of the machining system in the form of cutter radial and axial run outs. Moreover, the effect of instant tool tip displacements in axial and radial directions, caused by cutting forces, has been considered in the modeling procedure.

The proposed novel hybrid HMT/Z-Map 3D surface topography model applies the HMT and Z-map approaches in a specified modules. The HMT model is used to determine the position of the cutting edges. Information about the position of the cutting edges is necessary to determine the instant area of cut at time t and, consequently, to determine the components of the cutting forces. The Z-map model is used to create a model of the machined surface topography. The Z-map model employs the geometry outlined by subsequent cutting edges created in the HMT model. The outline of the proposed surface topography modelling procedure is presented in Figure 1.

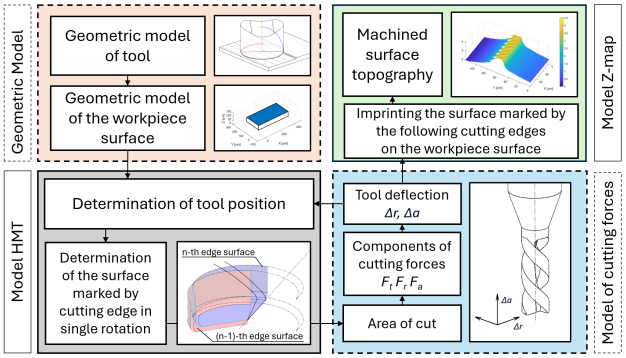


**Figure 1.** The outline of the proposed micromilling model

### *2.1. Geometric model*

Both the tool and the workpiece are modeled as discrete entities represented by point clouds. This approach provides a highly flexible framework for simulating the interaction between the tool and the material, particularly in processes like hybrid manufacturing. By discretizing the workpiece as a point cloud, the material is represented as a surface through which the tool moves, dynamically interacting with the modeled geometry. This representation not only captures the geometry of the workpiece but also facilitates the integration of additive and subtractive manufacturing models in a hybrid manufacturing context.

The tool model is also defined as a point cloud, with the geometry of the cutting edge constructed by identifying the intersection of the tool body with a plane inclined by the helix angle λ. The modeled cutting edge consists of three distinct areas: the face cutting edge, the cylindrical cutting edge, and the corner radius cutting edge. Each area is modeled separately to account for the unique geometry of the tool body in these regions. This segmentation allows for an accurate representation of the tool's cutting edge geometry, ensuring precise simulation of its interaction with the material.

By using point clouds to describe both the tool and the workpiece, the model can accurately simulate the material removal process at a micro-scale. Additionally, this discretized approach is well-suited for high-resolution analysis, enabling detailed studies of cutting mechanics and surface quality.

### *2.2. HMT model*

The position of the cutting edge at a given time t is determined using a homogeneous matrix transformation, incorporating both translation and rotation. The angular position of the cutting edge, denoted as $\varphi(t)$, the axial depth of cut (ap), and the tool's position in the XY - plane are key parameters in this transformation. The tool's center position along individual axes is described using x(t) and y(t) formulas. The position of the cutting edge at a single moment t is described by the formula (1).

$$Cutting\ Edge^T = CuttingEdge^T|_{t=0} \cdot \mathrm{R_z(t)} \cdot \mathrm{T\ (t)} \qquad (1)$$

To define the surface traced by a cutting edge during a single revolution, its position is evaluated at discrete time intervals. Between consecutive moments t and t+Δt, the cutting edge undergoes rotation around the tool axis and a change in the position of the tool center. This motion generates a trochoidal surface, which characterizes the trajectory of the cutting edge. As the cutting edge rotates, it creates a surface corresponding to the material removed during a single tool pass. The material removed is bounded by the surfaces formed during consecutive revolutions and further constrained by the workpiece geometry. Importantly, each surface is uniquely associated with an individual cutting edge rather than the entire tool. Consequently, the model constructs as many surfaces as there are cutting edges. The trochoidal surfaces traced by each cutting edge collectively define the material removal process. The surfaces traced by subsequent cutting edges are shown in Figure 2.

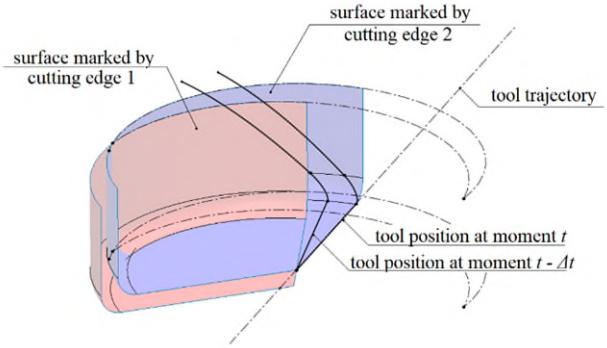


Figure 2. The surfaces traced by a following cutting edges

### *2.3 Model of cutting forces*

In order to estimate the instant cutting forces and tool tip displacements, the three coordinate systems ($XYZ$, TRA, $T_iR_iA_i$) were adapted in the modeling procedure. Each coordinate system (Fig. 3) is related to the geometry of the tool or workpiece and is used in the definition of force vectors.

In the XYZ system, the forces recorded by the dynamometer are determined. This is a system where the Z axis is consistent with the tool axis (assuming the tool is not tilted), X is the direction of feed movement, and Y results from the direction of the X and Z axes.

The TRA is a tool system. The zero point of the system is the tool tip, where the R axis lies in the radial direction, the A axis is consistent with the tool axis, while direction of the T axis results from the direction of the A and R axes. The TRA system rotates with the rotational movement of the tool. The values of the components of TRA cutting forces in the XYZ system are given by the equations (2) – (4).

$$F_X = F_T \cdot cos\varphi + F_R \cdot sin\varphi \qquad (2)$$

$$F_Y = -F_T \cdot sin\varphi + F_R \cdot cos\varphi \qquad (3)$$

$$F_Z = F_A \qquad (4)$$

The geometry of the cutting edge is given discreetly. The cutting edge is composed of a finite number of equally distributed $P_i$ points. Therefore, the $T_iR_iA_i$ system was defined separately at each point $P_i$ of the cutting edge. The direction of the $T_iR_iA_i$ system axis defines the directions of the vectors of the cutting force components $\hat{F}^{\lambda}_{t_i}$, $\hat{F}^{\lambda}_{r_i}$ and $\hat{F}^{\lambda}_{a_i}$. The axes directions depend on the position of the point $P_i$ on the defined cutting edge. The method of transforming the components of cutting forces from the $T_iR_iA_i$ coordinate system to the TRA system is shown by the formula (5)-(7).

$$F_T = F_{t_i} \cdot (cos\lambda_{\mathrm{eff}} \cdot cos\alpha_\lambda - sin\lambda_{\mathrm{eff}} \cdot sin\beta_\lambda \cdot sin\alpha_\lambda) + \\ + F_{r_i} \cdot (-cos\lambda_{\mathrm{eff}} \cdot sin\alpha_\lambda - sin\lambda_{\mathrm{eff}} \cdot sin\beta_\lambda \cdot cos\alpha_\lambda) + \\ + F_{a_i} \cdot sin\lambda_{\mathrm{eff}} \cdot cos\beta_\lambda \qquad (5)$$

$$F_R = F_{t_i} \cdot cos\beta_\lambda \cdot sin\alpha_\lambda + F_{r_i} \cdot cos\beta_\lambda \cdot cos\alpha_\lambda + \\ + F_{r_i} \cdot cos\beta_\lambda \cdot cos\alpha_\lambda + \\ + F_{a_i} \cdot sin\beta_\lambda \qquad (6)$$

$$F_A = F_{t_i} \cdot (sin\lambda_{\mathrm{eff}} \cdot cos\alpha_\lambda - cos\lambda_{\mathrm{eff}} \cdot sin\beta_\lambda \cdot sin\alpha_\lambda) + \\ + F_{r_i} \cdot (-sin\lambda_{\mathrm{eff}} \cdot sin\alpha_\lambda - cos\lambda_{\mathrm{eff}} \cdot sin\beta_\lambda \cdot cos\alpha_\lambda) + \\ + F_{a_i} \cdot cos\lambda_{\mathrm{eff}} \cdot cos\beta_\lambda \qquad (7)$$

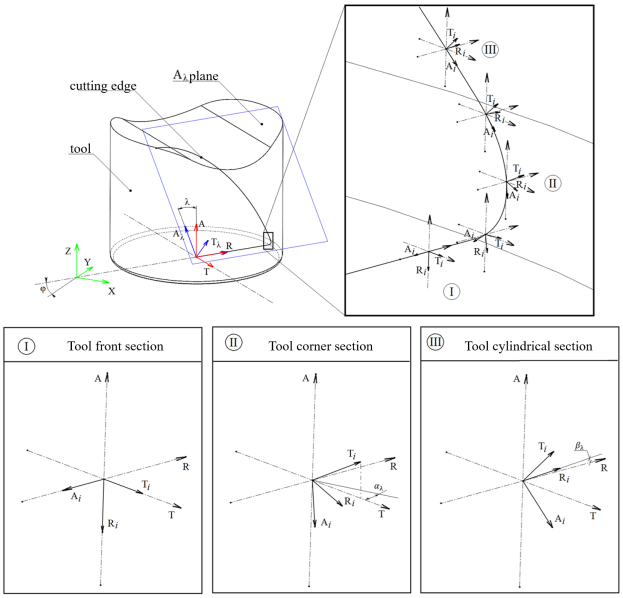


**Figure 3** The coordinate systems adapted in the modeling procedure of force and displacements

The directional vectors of the forces in the $T_iR_iA_i$ coordinate system can be denoted as $\hat{F}^{\lambda}_{t\ i}$, $\hat{F}^{\lambda}_{r\ i}$, $\hat{F}^{\lambda}_{a\ i}$. These vertices can be determined by three support vectors: $\hat{s}_i$ - the vector tangent to the cutting edge line at point $P_i$, $\hat{v}_{r_i}$- the peripheral velocity vector at point $P_i$ and $\hat{x}_{\gamma_i}$ - vector lying on the rake face at point $P_i$ (assuming $\gamma = 0$). The method of determining the force verses in the $T_iR_iA_i$ system is shown in formulas (8) – (10).

$$\hat{F}^{\lambda}_{t\ i} = \frac{\hat{s}_i \times \hat{x}_{\gamma_i}}{|\hat{s}_i \times \hat{x}_{\gamma_i}|} \tag{8}$$

$$\hat{F}^{\lambda}_{r\ i} = \hat{x}_{\gamma_i} \tag{9}$$

$$\hat{F}^{\lambda}_{a\ i} = -\hat{s}_i \tag{10}$$

### *2.4 Iterative algorithm of tool deflection*

The values of deflections in axial Δa and radial Δr directions were determined by the iterative algorithm. In each iteration, the determined elementary deflection (dr and da) is introduced in the direction that leads to the equilibrium state. After entering the elementary deflection, a new position of a tool is determined. The change in the position of the tool introduced in this way results in a reduction of the area of cut (and uncut chip thickness). Then, new values of cutting forces acting in $T_iR_iA_i$ system are determined. In the new position of the tool, the elastic forces are being calculated again. When conditions are not met in this iteration, algorithm moves to next iteration. The resultant forces $F_{Rj}$, $F_Aj$ in the j-th iteration are determined by summing the values of $F_{Ri}$, $F_{Ai}$ forces at all points $P_i$ where k is the number of points $P_i$. The values of the elastic forces in the j-th iteration $F_{krj}$, $F_{kaj}$ are determined using the equations (11, 12), where $F_{Rm}$, $F_{Am}$, $F_{krm}$, $F_{kam}$ are the values of the forces in the m-th iteration.

$$F_{krj} = k_r \cdot \sum_{m=1}^{j-1} \left( \frac{(F_{Rm} - F_{krm})}{|F_{Rm} - F_{krm}|} \cdot dr \right) \tag{11}$$

$$F_{kaj} = k_a \cdot \sum_{m=1}^{j-1} \left( \frac{(F_{Am} - F_{kam})}{|F_{Am} - F_{kam}|} \cdot da \right) \tag{12}$$

The algorithm runs until an equilibrium state is found in both directions. The deflection of the tool in the equilibrium state obtained in the j-th iteration is determined using the equations (13), (14).

$$\Delta r = \sum_{i=1}^{j} \frac{(F_{Ri} - F_{kri})}{|F_{Ri} - F_{kri}|} dr \tag{13}$$

$$\Delta a = \sum_{i=1}^{j} \frac{(F_{Ai} - F_{kai})}{|F_{Ai} - F_{kai}|} da \tag{14}$$

The equilibrium condition in i-th iteration is satisfied when the difference of the elastic force of the tool ($F_{kri}$, $F_{ari}$) and the corresponding component of the cutting force ($F_{Ri}$, $F_{Ai}$) are equal in both directions.

### *2.5 Z-map model*

The surface created by the cutting edge is generated through its successive positions, forming a radial mesh without predefined nodes. The positions of these nodes are determined dynamically by the cutting edge's location at each moment. As a result, the mesh of the traced surface differs from that of the workpiece. To accurately model the surface traced within the workpiece, the nodes of the traced surface's mesh must be dynamically adjusted.

The mesh of the workpiece is predefined, characterized by a regular structure with adjustable density. Consequently, the mesh corresponding to the cutting edge is interpolated to align with the predefined workpiece mesh.

Having a surface traced by the cutting edge described on the same mesh as the workpiece, the Z-map model is being used. The Z-map model is based on comparing geometry values in the corresponding nodes of two meshes. One of the meshes is a modified mesh and the other is a modifying mesh. In the presented case, the modified geometry is the workpiece material, while the modifying geometry is the mesh of the surface traced by the cutting edge.

If the value at the modified geometry node is greater than the value at the modifying geometry node, the modified geometry takes on the value of the modifying geometry. However, if the modifying geometry's value is greater, the modified geometry retains its original value.

## 3. Micromilling anomalies mechanism

Micromilling experiments were conducted on the Inconel 718 alloy. Its strength and durability are largely attributed to its alloying elements, including nickel (50%), chromium (17%) and niobium (5%), which increase its resistance to high-temperature deformation and oxidation. Area of 6 mm x 7 mm were sectioned off on the fabricated workpiece. In the conducted cutting tests with ae = 300 µm, fz = 3 µm, 15 passes of the tool were carried out with the set parameters.

During micromilling, the monolithic micro end mills JS512015F2C.0Z2 made of sintered carbide with NXT anti-wear coatings were applied. The micromilling tool had the nominal diameter D = 1.5 mm.

The radial stiffness of the tool was determined experimentally. The displacement was initiated by rigid steel block attached to the moving machine table. The displacement was forced in steps, every 1 µm. The tool tip was supported on a movable block with a cylindrical surface. The determined stiffness in radial direction took the value $k_r$ = 0.27 N/µm.

During the evaluation of axial stiffness, the system was modeled as three elastic elements connected in series. The stiffness of the first element $k_1$ replaces the stiffness of the

milling tool, while the stiffness of the second element $k_2$ replaces the stiffness of the workpiece. The stiffness of the third element $k_o$ replaces the stiffness of the tool in the working part section. The summed stiffnesses $k_1$ and $k_2$ were determined experimentally by pressing the cutter shank into the workpiece material and measuring the force at the defined translation. The $k_o$ stiffness was determined using the finite element method. The determined axial stiffness of the system is $k_a$ = 0.56 N/µm.

Regularly occurring bands were observed, characterized by a reversal in the direction of traces left by the cutting edge. The regions exhibiting this reversed feed mark direction were elevated (Fig. 4). Simulations using presented model were performed using identical parameter values (Fig.5).

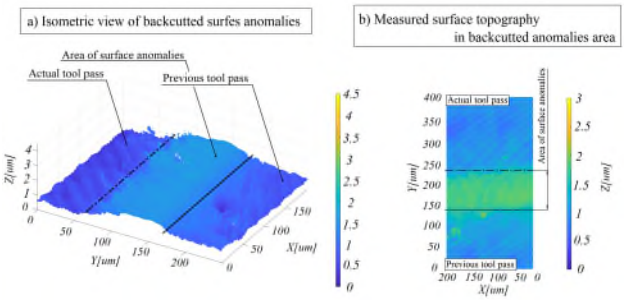


**Figure 4.** Machined surface a) isometric view; b) marked observed bound

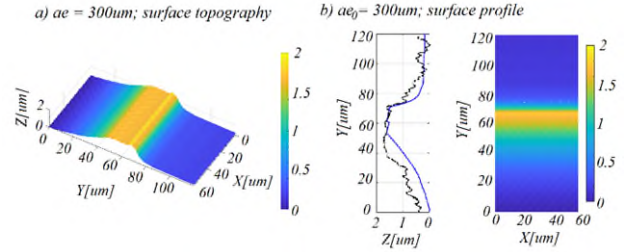


**Figure 5.** Modelled surface a) isometric view; b) comparison of modelled and experimental surfaces profiles

During down-micromilling process conducted with micromills with a helical cutting edges (λ ≠ 0), the cutting action (defined as an engagement of a cutting edge into the workpiece) takes place gradually. Consequently, the values of active length of cutting edge and instant axial depth of cut ap(φ) grow with an increase of tool rotation angle φ. Therefore, two distinct stages of tool immersion into the workpiece, diversified in terms of instant axial depth of cut ap(φ) can be distinguished (Fig. 6). In the first stage, the ap(φ) < ap, which means that only some part of an active cutting edge length is engaged in the micromilling process. In the second stage (Fig. 6b), the ap(φ) = ap, which means that the micromilling process takes places with a defined cutting parameters and corresponding active length of cutting edge.

Taking into the consideration the micromilling cases investigated in this study (axial depth of cut equal to 100 µm and higher than tool corner radius rε = 28 µm, down-milling), during the first stage of tool – workpiece engagement (ap(φ) < ap), and when the ap(φ) ≤ rε, the resultant instantaneous thrust force has a positive sign, which means that the flexible tool is being elevated towards the workpiece (Fig. 6a). As a consequence, cutting edge trajectory is being elevated vertically, which in turn relocates on the machined surface topography and contributes to a formation of machined surface anomalies in a form of the region with the elevated machining marks towards the remaining area. Tool's axial deflection shown in Fig. 6c i9s a result of changing cutting force and it is reflected in surface profile.

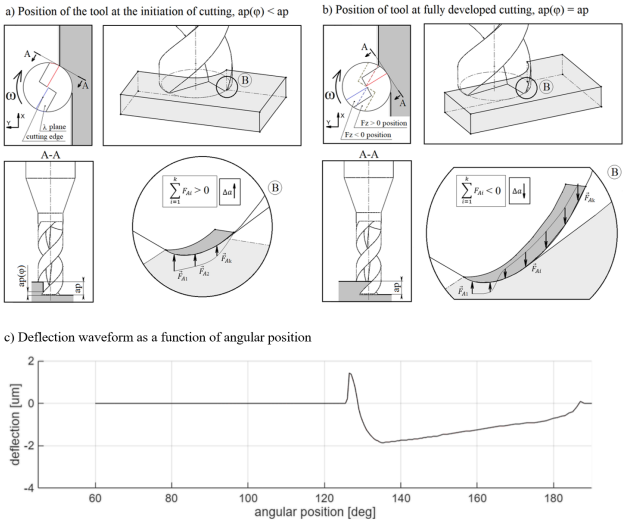


**Figure 6.** Workpiece engagement and resultant thrust forces distributed on the micromilling tool: a) ap(φ) < ap ; b) ap(φ) = ap; c) deflection of the tool as a function of angular position

## 4.Conclusions

In this work a novel surface topography model intended for radial immersion micro end milling has been proposed. The developed model has been successfully validated during micromilling experiment of Inconel 718 alloy, involving a 3D inspections of a milled surfaces. Based on the conducted simulations and experiments the following conclusions can be formulated:

(a) During down-micromilling process conducted with micromills equipped with a helical cutting edges (λ ≠ 0) and corner radius (rε > 0), the formation of machined surface anomalies in a form of the region with the elevated machining marks towards the remaining area is observed. These anomalies are directly induced by the force/tool deflection variations

(b) The formulated original 3D surface topography model based on a hybrid HMT/Z-Map approach, concerning trochoidal trajectory of tool, tool run-out and tool tip deflections in radial and thrust directions enables accurate estimation of geometrical parameters (heights and widths) of surface anomaly bands in a wide range of machining conditions and tool geometries.

Future work could focus on refining the selection of micromilling parameters and tool geometry to minimize surface anomalies, particularly in down-micromilling. This includes exploring optimal combinations of radial depth of cut, feed per tooth, tool helix angle, and corner radius. Additionally, further investigation into the impact of micromilling kinematics (up-milling vs. down-milling) is warranted, as initial findings suggest that up-micromilling kinematics prevent the formation

## References


[1] Wang D, Ren J and Tian W 2020 A method for the prediction of cutting force for 5-axis ball-end milling of workpieces with curved surfaces *Int. J. Adv. Manuf. Technol.* **107** 2023-39

[2] Mann B P, Edes B T, Easley S J, Young K A and Ma K 2008 Chatter vibration and surface location error prediction for helical end mills. *Int. J. of Machine Tools and Manufacture* **48**, 350-61

[3] Wojciechowski S, Krolczyk G M and Wiąckiewicz M 2018 Study on metrological relations between instant tool displacements and surface roughness during precise ball end milling *Measurement* **129** 686-94

[4] Grossi N, Scippa A, Sallese L, Montevecchi F and Campatelli G 2018 On the generation of chatter marks in peripheral milling: A spectral interpretation *Int. J. of Machine Tools and Manufacture* **133** 31-46

[5] Kalinski K J and Galewski MA 2015 Optimal spindle speed determination for vibration reduction during ball-end milling of flexible details *Int. J. of Machine Tools and Manufacture* **92** 19-30